Korean J. Chem. Eng., 38(12), 2468-2478 (2021)
DOI: 10.1007/s11814-021-0890-5

pISSN: 0256-1115
eISSN: 1975-7220

Highly efficient bi-metallic bismuth-silver doped TiO_2 photocatalyst for dye degradation

Nandana Chakinala*, Parag Ratnakar Gogate, and Anand Gupta Chakinala*,†**

*Department of Chemical Engineering, Manipal University Jaipur, Dehmikalan, Jaipur-303007, Rajasthan, India
**Department of Chemical Engineering, Institute of Chemical Technology, Mumbai-400019, Maharashtra, India
(*Received 29 April 2021 • Revised 14 June 2021 • Accepted 2 July 2021*)

Abstract−Several mono-and bi-metallic photocatalysts with different loadings have been synthesized using ultrasound assisted sol gel and wet impregnation methods. Synthesized catalysts were characterized using various analytical techniques to determine the bandgap, functional groups, crystallinity, and surface morphology. Photocatalytic performance of the different catalysts was compared in terms of Rhodamine-B dye degradation, and further process optimization studies were carried out to achieve the maximum extent of degradation. Catalyst performance was studied both under UV and visible light irradiation for the degradation of different dyes. Compared to pure TiO_2 and monometallic Ag or Bi doped on TiO_2, bi-metallic Bi-Ag on TiO_2 catalyst synthesized using wet impregnation was found to be highly active under the conditions investigated. Complete degradation (~100%) was obtained within shorter duration in the presence of minimal catalyst loading (60 mg/L). Overall, this work has clearly demonstrated the higher catalytic activity of bi-metallic catalyst, which is attributed to the synergistic effect of Bi and Ag on TiO_2 facilitating the efficient charge separation and improved e^- transfer combined with high ability to absorb in visible light region in effectively degrading organic pollutants.

Keywords: Photocatalysis, Bi-metallic Catalysts, Dye Degradation, Rhodamine-B, Bismuth

INTRODUCTION

Due to rapid industrialization and urbanization, there is an increasing environmental concern particularly related to pollution of water bodies, mainly in the developing countries causing severe health issues. Though there are several best available technologies for the treatment of industrial wastewater, they are expensive both in-terms of capital and operating costs and being less effective in the treatment [1]. Hence, there is a growing need for the development of low-cost treatment technologies. Advanced oxidation processes (AOP) like photocatalytic treatment have gained interest owing to its effectiveness in degradation of wide variety of organics and dyes. It is an economical and greener process for the treatment of wastewater carried out at milder conditions [2,3]. In this process, the catalyst plays a vital role in deciding the efficiency of photodecomposition/photo-oxidation. TiO_2 is extensively used for the photocatalytic degradation of various organic and inorganic pollutants due to several benefits, such as low price, availability, low toxicity, and high activity/stability [4]. However, the expansive band gap (E_g=3.2 eV) restricts its application in the solar spectrum (3-5%). It is imperative to develop novel catalysts that are active and stable in visible light conditions having lower band gap. Development of highly efficient photocatalysts is aimed towards increasing the photocatalytic activity by doping it with other semiconductor materials, transition elements and noble metals [5]. This method of doping is found to enhance the degradation efficacy by improving the optical properties associated with photocatalytic activity, and by extension to the visible region thereby reducing the recombination of electrons and holes [6-9].

Among several catalysts reported in the literature, silver doped TiO_2 catalysts have been extensively studied with demonstrated high photocatalytic activity for the degradation of several organic contaminants [7,8,10,11]. The doping of optimum amounts of silver on TiO_2 improves its absorption properties and reduces the bandgap promoting the photocatalytic activity [10]. Bismuth-based nanomaterials have also gained considerable attention due to their low cost, non-toxicity, high stability and high photocatalytic activity [12]. Bismuth oxide families of nanomaterials and doped catalysts have been reported to be highly photoactive in visible light for the efficient degradation of several organics due to excellent absorption ability as well as effective charge separation [4,9,13-15]. Moreover, co-doped Bi with other dopants have also shown to improve the photocatalytic activity toward efficient degradation of pollutants due to the synergistic effects of different metals. Doping of Bi introduces an energy level below the conduction band that leads to enhanced absorption in the visible light region due to reduced band gap.

More recently, heterojunction nanocomposites based on Z-scheme photocatalysts have been extensively studied for photodegradation of dyes owing to their high ability of photo absorption as well as strong redox ability to drive photoreactions. Plasmonic Z-scheme structure nanocomposite catalysts based on silver and bismuth were found to exhibit high photocatalytic efficiency for the degradation of dyes [16-20].

The studies reported to date in the literature have shown complete degradation of dyes though with large amounts of catalysts and

†To whom correspondence should be addressed.
E-mail: anandgupta.chakinala@jaipur.manipal.edu, a.g.chakinala@gmail.com

Table 1. List of different synthesized catalysts

Sl. No.	Catalyst ID	Catalyst composition	Synthesis procedure
1	Cat-A	0.5%Bi-0.5%Ag/TiO_2	US -SG
2	Cat-B	0.5%Bi-0.5%Ag/TiO_2	US-WI
3	Cat-C	0.75%Bi-0.25%Ag/TiO_2	US-WI
4	Cat-D	0.25%Bi-0.75%Ag/ TiO_2	US-WI
5	Cat-E	1.5%Bi/TiO_2	US-SG
6	Cat-F	1.0%Bi/TiO_2	US-WI
7	Cat-G	1.0%Ag/TiO_2	US-WI
8	Cat-H	1.5%Bi/TiO_2	US-WI
9	Cat-I	1% Ag/TiO_2	US -SG

longer reaction times under visible/UV light irradiation. The present study is aimed at the synthesis of different mono- and bi-metallic doped TiO_2 photocatalysts *via* ultrasound assisted sol-gel and ultrasound assisted wet impregnation methods for its application in dye degradation. In the present study, we focussed on the minimal metal loadings for a reduced catalyst cost and studied their photocatalytic behavior for Rh-B dye degradation. The best catalyst screened was further optimized in detail and studied intensively.

EXPERIMENTAL

In this work, several photocatalysts were synthesized *via* ultrasound assisted sol-gel technique (US-SG), and ultrasound assisted wet impregnation technique (US-WI). All the catalysts synthesized were tested for degradation of different dyes as Rhodamine-B (Rh-B), Methylene Blue (MB), Congo Red (CR) and Rhodamine-6G (Rh-6G) under UV irradiation and sunlight.

1. Chemicals and Materials

Titanium isopropoxide precursor was procured from Sigma Aldrich. Other chemicals like ethanol, nitric acid, silver nitrate, bismuth subnitrate, and different dyes (Rh-B, MB, CR, Rh-6G) were procured from Loba Chemie. Titanium dioxide was procured from Merck Life Sciences Private Limited. All the chemicals were of synthesis grade with high purity (>98%) and used as received from the supplier. Distilled water was used in all the catalyst synthesis methods.

2. Catalyst Synthesis Procedure

2-1. US-SG

Silver nitrate, bismuth subnitrate and titanium isopropoxide were used as precursors and ethanol was used as solvent. In ultrasound assisted synthesis procedure [21], 10 mL of titanium isopropoxide and 30 mL of ethanol were mixed and stirred continuously for 15 min, which is referred to as solution-A. HNO_3 solution was prepared by mixing 0.1 mL HNO_3, 20 mL ethanol and 1 mL water, which is referred to as solution-B. The prepared solution-B was added dropwise to solution-A under continuous stirring. The mixture was subjected to homogenization for 30 min followed by sonication in an ultrasound bath (LMUC-12, Labman Scientific Instruments, 300 W, 40 KHz) for 30 min. Water was added dropwise until gel formation occurred. The obtained gel was dried at 100 °C for 12 h followed by calcination at 400 °C for 2 h. For preparing metal doped TiO_2, appropriate quantities of metal precursors were added to the solution under stirring.

2-2. US-WI

In the wet impregnation method [8], 3 g of synthesis grade titanium oxide was mixed with 30 mL ethanol under continuous stirring. Appropriate amounts of metal precursors were added gradually to the solution under stirring. The prepared solution was subjected to sonication for 1 h. The resulting solution was rested overnight, and then ethanol was evaporated by drying at 100 °C for 12 h. The dried catalyst was crushed and calcined at 400 °C for 2 h. The catalysts synthesized using different approaches and with different metal loadings are given in Table 1.

3. Experimental Setup and Procedure

The photocatalytic activity of the synthesized catalysts was compared for the degradation of Rh-B dye. The experiments were carried out in a 500 mL laboratory scale photocatalytic reactor equipped with 250 W UV lamp. The set-up consists of a central double water jacket through which water is circulated to protect the lamp from overheating. A specific amount of catalyst (30 mg) was added to 500 mL of Rh-B dye solution and the mixture was stirred in the dark at 800 rpm for 30-40 min to attain the adsorption equilibrium. Later, the mixture was irradiated with the UV lamp at constant stirring speed and the samples were withdrawn from the reactor at regular time intervals. The samples were filtered through a 0.2-micron filter followed by centrifuge at 4,500 rpm for 5 min. The supernatant liquid was analyzed for its absorbance using a UV-Vis spectrophotometer (HACH-DR 6000). As the wavelength of maximum absorbance of the dye was found to be 555 , the absorbance data for all the samples were recorded at the same wavelength. All the experiments were carried out at a pH of 7 (unless specified) and the temperature was maintained at 25±3 °C. Rh-B dye concentration was determined using the calibration plot at 555 nm. Complete wavelength scans of other dyes such as MB, Rh-6G, CR that are studied under visible light conditions were performed to identify the maximum absorption wavelength. The degradation rates of these dyes were then estimated at their maximum absorbance (MB: 664 nm; Rh-6G: 525 nm CR: 497 nm). Visual observations and snapshots of samples taken at different time intervals were inspected and discussed qualitatively with respect to their decolorization. The initial pH of feed solutions was adjusted with dilute HCl or NaOH solution.

Visible light experiments were conducted with 10 ppm solutions of different dyes (Rh-B, Rh-6G, MB, CR) exposed to sunlight with

temperature in the range of 20-25 °C at open space (26°50′36″N; 75°34′1″E) during 10:00 AM-2:00 PM with continuous stirring at 800 rpm after attaining the adsorption equilibrium. The percentage dye degradation is calculated as given below.

$$\text{Dye degradation (\%)} = \left(1 - \frac{C}{C_o}\right) \times 100 \quad (1)$$

where C_o and C are the dye concentration in water at time t=0 (after adsorption equilibrium) and t=t, respectively. Initial tests were done to check the repeatability in which tests were performed at identical conditions in triplicates and the results were reproducible having a confidence interval of >95%.

4. Catalyst Characterization

The calcined materials were characterized using different analysis techniques such as Fourier transform infrared spectroscopy (FTIR), ultraviolet-visible spectroscopy (UV-vis), photoluminescence (PL), field emission scanning electron microscopy (FESEM) and X-ray diffraction analysis (XRD). FTIR spectra were obtained between 500 to 4,000 cm^{-1} on a Bruker-Alpha instrument equipped with zinc selenide ATR crystal plates at a resolution of 0.8 cm^{-1}. The diffuse reflectance spectra of the samples were analyzed in the wavelength range of 200-900 nm using Shimadzu UV-2600 spectrophotometer consisting of double beam photometric system. The reflectance data was further converted to parameter F(R), that is proportional to molar absorption coefficient and scattering factor, using inbuilt Kubelka-Munk model. The photoluminescence (PL) spectra of the powder samples were recorded using Horiba FluoroMax-4 spectrometer with an integration time of 5 s at 30°. The FESEM analysis of the solid samples was carried out using the JEOL make JSM-7610 FPlus fitted with energy dispersive X-ray (EDX) detector for elemental analysis at the micro-nanoscale. The samples were analyzed directly without any sputter coating as they are semi-conducting. The powder XRD analysis was carried out using Xpert3 Pan-analytical instrument.

RESULTS AND DISCUSSION

1. Catalyst Characterization

1-1. FTIR Analysis

FTIR analysis of the prepared photocatalysts was performed to establish the key functional groups and the obtained spectra are shown in Fig. 1. It is observed that all the catalysts synthesized via wet impregnation method exhibited a peak at 742-777 cm^{-1} due to the O-Ti-O bonding in anatase structure, which is not observed in the catalysts synthesized by sol-gel method [4]. Besides this, spectra of all catalysts exhibited similar absorption peaks in the regions at 524-544, 1,500-1,700, 2,360, 3,745 and 3,854-3,899. The peaks at 524 cm^{-1} show stretching vibration of Ti-O-Ti and the peaks above 3,700 correspond to OH stretching vibration due to presence of hydroxyl groups [22]. All the catalysts had two medium bands in 1,500-1,700 cm^{-1} which is due to the deformation vibration of adsorbed water molecules. It was reported that with an increase in Bi loading the amount of surface adsorbed water and hydroxyl groups increased, which are bound to react with the valence band photo induced holes producing free radicals which aid in improving the photocatalytic activity [4]. In addition, the absence of any peak around 1,200 cm^{-1} was also attributed to the metal doping inside the TiO_2 lattice [23].

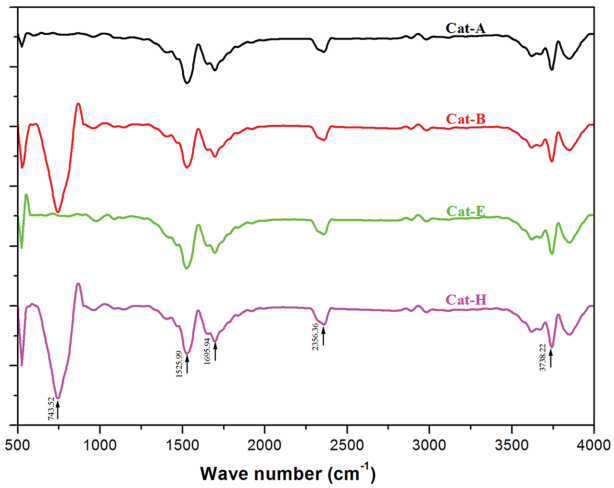

Fig. 1. FTIR spectrum of the photocatalysts synthesized using US-SG and US-WI.

1-2. Diffuse Reflectance Spectra (DRS) Analysis

Optical absorption properties of pure and doped TiO_2 photocatalysts were studied using UV-vis spectrometer in diffuse reflec-

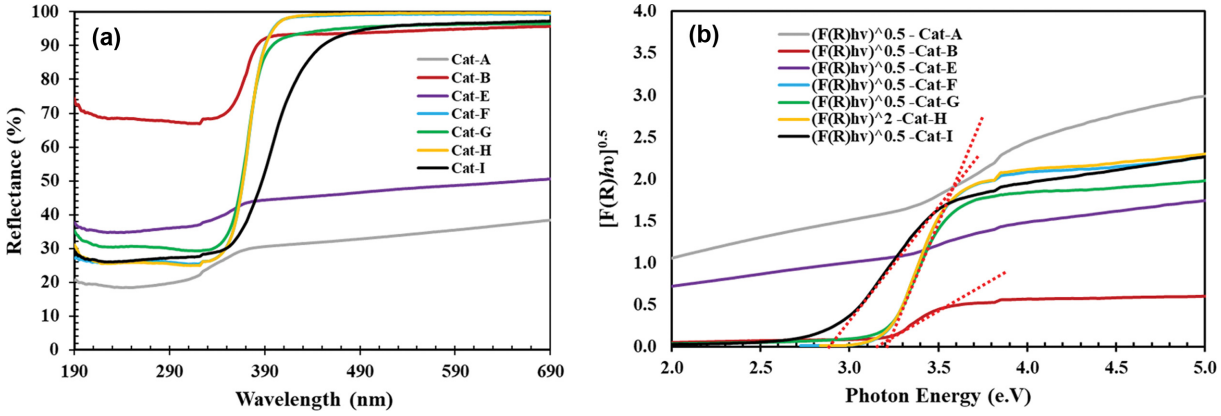

Fig. 2. (a) UV-Vis diffuse reflectance spectra and (b) band-gap energy analysis.

Table 2. Summary of catalyst performance for Rh-B dye degradation

Sl. No.	Catalyst ID	Degradation (%)*	Rate constant $k_{app}\times10^2$, min^{-1}	R^2 (-)	Band gap (eV)
1	Cat-A	86	3.53	0.995	2.70
2	Cat-B	99 (Clear liquid in 30 min)	11.76	0.993	3.15
3	Cat-C	92	4.61	0.997	3.20
4	Cat-D	98	8.20	0.980	3.20
5	Cat-E	92	4.54	0.993	3.20
6	Cat-F	82	3.48	0.994	3.20
7	Cat-G	97 (Clear liquid in 40 min)	9.14	0.988	3.20
8	Cat-H	98	6.52	0.997	3.20
9	Cat-I	87	3.60	0.997	2.90
10	TiO_2	82 (in 50 min)	3.46	0.980	3.20
11	No catalyst	70	2.25	0.983	-

*Note: Reported degradations are achieved in 1 h duration unless specified.

tance mode [24]. Fig. 2(a) depicts the UV-vis diffuse reflectance spectra of the pure and doped photocatalysts. It is evident that after doping with silver and bismuth, the response of photocatalysts has shown minimal changes in the peak shifts, resulting in slight reduction of band gap energy. The DRS data were analyzed using Kubelka-Munk equation as given below to estimate the Kubelka-Munk function parameter F(R) [24].

$$F(R)=\left[\frac{(1-R^2)}{2R}\right] \quad (2)$$

R is the measured absolute reflectance of the photocatalyst. Fig. 2(b) presents the Kubelka-Munk plots for pure and doped photocatalysts. Kubelka-Munk plots of $[F(R)*h\upsilon]^{0.5}$ vs $(h\upsilon)$, where $h\upsilon$ is the photon energy, were used to determine the band gap energy (E_g), which is the intercept value of the extrapolated linear part of the plot. The band gap energies of synthesized catalysts are summarized in Table 2. Minimal changes in the band gap energies were observed due to substantially lower metal loadings used in this study, which is evident from Fig. 2(b). The band gap values of bimetallic Cat-B were found to be relatively lower ~3.15 eV when compared to the pure TiO_2 with ~3.2 eV.

1-3. Photoluminescence Spectra Results

Photoluminescence (PL) analysis of the catalysts was carried out to understand the photocatalytic activity behavior that can be affected by recombination rate of charge carriers (e^-/h^+ pair). It is known that as the electrons and holes recombine, they emit photoluminescence proportional to the recombination rate. This analysis helps in estimating the efficiency of charge carrier separation in semiconducting materials. The higher PL intensity indicates a faster recombination rate of electron-hole (e^-/h^+) pairs, while lower intensity indicates reduced e^-/h^+ pair recombination rate. Fig. 3 shows the PL emission spectra (300-600 nm) of various catalysts confirming that the PL intensities of doped TiO_2 are lower than pure TiO_2, which is attributed to reduced recombination of charge carriers that enhances the photocatalytic activity. It is observed that the PL intensity of mono metallic catalysts (Cat-F, Cat-G and Cat-I) was lower compared to other synthesized catalysts.

1-4. Morphology Studies

The texture and morphology of the synthesized photocatalysts

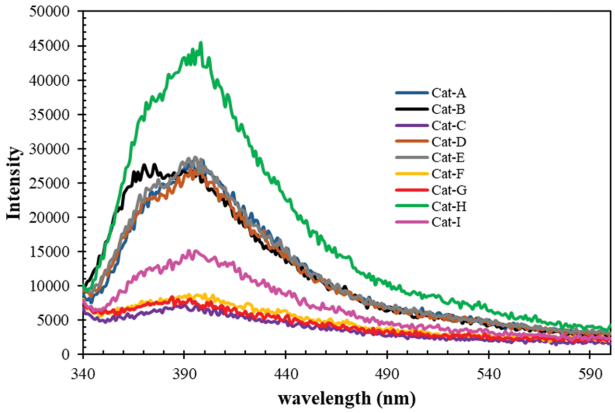

Fig. 3. PL spectra of photocatalysts.

were analyzed using FESEM. The results obtained are represented for CAT-A and CAT-B as shown in Fig. 4. The surface morphology of the catalysts synthesized using sol-gel process was irregular in shape with different sizes in micron range, which may lead to improper distribution of active metals. Catalysts synthesized using wet impregnation were found to have a more uniform and spherical shape with typical sizes in the range of 200-300 nm, facilitating a better distribution and accessibility of active metals on the surface. Since the metal loadings were very low, it did not significantly affect the texture and morphology of the catalyst. The EDX analysis confirmed the elemental composition of the metal loadings on the TiO_2, which were found to be in line with the actual metal loadings used in the preparation.

1-5. XRD Analysis

XRD analysis of Cat-A and Cat-B is shown in Fig. 5 which compares the different synthesis methods of sol gel and wet impregnation. The XRD results of other catalysts were not shown as the peaks were identical depending on the synthesis methods used. It is evident from the figure that the catalysts exhibited anatase phase of TiO_2 without any other phases or impurities pertaining to the dopants. Since the amount of metal loading is very low it is unlikely in the detection limits of XRD, and the active metals may successfully be doped into the lattice of the TiO_2, or they could be well

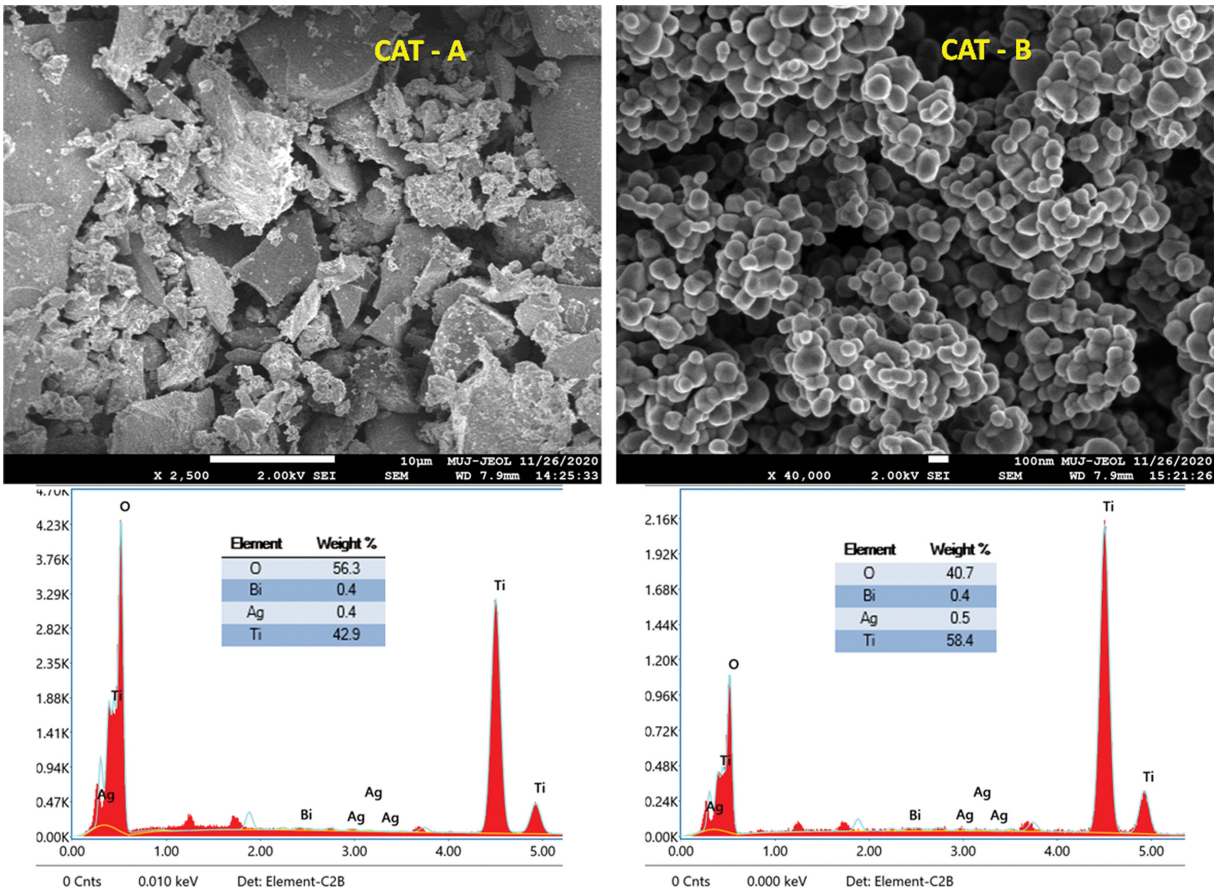

Fig. 4. Surface morphology and elemental analysis of Cat-A and Cat-B.

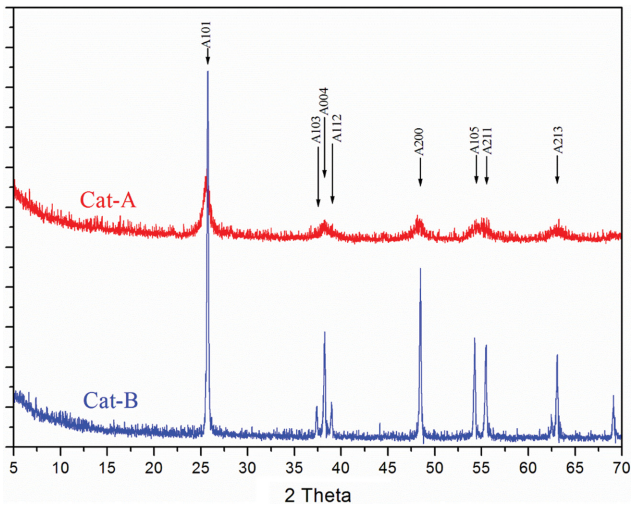

Fig. 5. XRD patterns of CAT-A and CAT-B.

dispersed on the surface. Doping of metals such as Bi and B on TiO_2 was reported to inhibit the anatase particle growth [4]. On the other hand, doping high amounts of Ag on TiO_2 promotes crystallization of anatase to rutile phase [10]. In the case of catalysts prepared by US-WI, the samples showed XRD patterns with major diffraction peaks 2θ=25.3°, 37°, 37.7°, 38.5°, 48.1°, 53.8°, 55.1°, 62.6°, and 68.6° corresponding to (1 0 1), (1 0 3), (0 0 4), (1 1 2), (2 0 0), (1 0 5), (2 1 1), (2 1 3), and (1 1 6) confirming the presence of anatase phase. In the case of catalysts prepared by US-SG, the peaks at 2θ=37, 38.5, 68.6 were missing, implying the reduction of anatase phase. Moreover, the intensity of the peaks was higher in the case of wet impregnation method as shown in Fig. 5, which is attributed to the fact that the method of catalyst synthesis not only affects the crystal growth but also the crystal structure. Higher peak intensities indicate that the anatase phase of TiO_2 is more crystalline. It was also reported that anatase phase of synthesized TiO_2 has higher photocatalytic activity as compared to other crystalline phases (rutile and brookite) [25]. A broader peak was observed in the XRD spectrum of CAT-A at 53.8° instead of two different peaks at 53.8 and 55.1 in CAT-B, which can be due to the difference in the crystallite size [25].

2. Photocatalytic Activity

2-1. Kinetic Analysis of Rh-B Degradation

A kinetic study of Rhodamine-B dye degradation under UV and visible light irradiation was carried out, using Langmuir-Hinshelwood (L-H) model that is widely used to represent heterogeneous kinetics [26]. It relates the degradation rate of an organic pollutant with respect to its concentration, which is expressed as follows:

$$-r_i = \frac{dC_i}{dt} = \frac{k_r K_{ads} C}{1 + K_{ads} C} \quad (3)$$

where k_r is the intrinsic rate constant (min^{-1} mg L^{-1}), K_{ads} is the adsorption equilibrium constant of dye on the catalyst surface (mg^{-1} L), C is the dye concentration in water (mg L^{-1}) and t is irradiation time (min). For lower rates of adsorption and low concentration of dye (K_{ads}.C<<1), the equation is simplified to first-order kinetic model, which on integration gives the expression for concentration at time with an apparent first-order rate constant k_{app} (min^{-1}) as shown below.

$$\ln\left(\frac{C}{C_o}\right) = -k_r K_{ads} t = -k_{app} t \quad (4)$$

A plot of $-\ln(C/C_o)$ vs. t gives a straight line, from which k_{app} is obtained as slope of the plot. Table 2 lists the k_{app} values of Rh-B dye degradation in a photocatalytic reactor using different synthesized catalysts under UV irradiation. The correlation coefficients R^2 indicate that the first-order degradation kinetics resulting from L-H model adequately fits the experimental data.

2-2. Catalyst Screening Studies

The photocatalytic activity of several synthesized catalysts was investigated under identical conditions for the degradation of Rh-B dye in a photocatalytic reactor; and a summary of degradation achieved with apparent rate constants is shown in Table 2. It can be seen that the degradation in the absence of catalyst was only ~70%, which increased to ~82% in the presence of TiO_2. All synthesized catalysts with US-SG and US-WI approaches were seen to be more active (>90% degradation achieved) for the Rh-B dye degradation. However, among the catalysts studied a colorless solution was obtained with Cat-B and Cat-G within 30 and 40 min, respectively.

It was also inferred that the photocatalytic activity of bimetallic Bi-Ag/TiO_2 (CAT-B) synthesized *via* US-WI was higher compared to all other catalysts synthesized using US-SG. Complete discoloration of the dye was observed in less than 30 min using CAT-B, whose photocatalytic activity is analogous to 1% Ag/TiO_2 (Cat-G) as shown in Fig. 6. Similarly, the photocatalytic activity of bimetallic Bi-Ag/TiO_2 (Cat-A) is in-line with 1% Ag/TiO_2 (Cat-I). These results suggest that Ag can be partly replaced with Bi without compromising on the photocatalytic activity. The US-WI catalysts were found to be very well dispersed in the feed solution compared to the US-SG catalysts that could probably lead to high quantum efficiency. Note that significant degradation was achieved with much less amount of catalyst loading (60 mg/L) compared to other studies reported in the literature (Table S1).

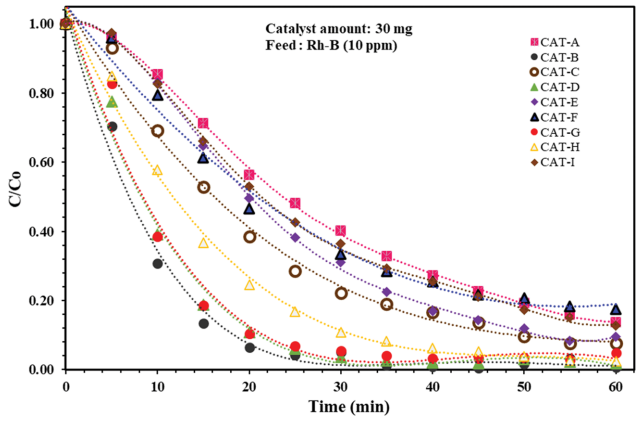

Fig. 6. Comparison of photocatalytic activity for bimetallic and monometallic catalysts.

The effect of three different bi-metallic catalyst loadings (Cat-B, Cat-C, Cat-D) was also studied by varying the proportions of Bi and Ag within the limit of 1 wt% of total metal loadings on TiO_2. It is observed that the effect of silver is more pronounced in the bimetallic catalyst and increasing the bismuth proportion beyond 0.5% reduced the degradation. An optimum ratio of 0.5 : 0.5 wt% of Bi and Ag was found to result in high activity. To understand the effect of bismuth alone, tests were also carried out with different Bi loadings of 1 and 1.5 wt%. From Fig. 6, it is observed that by increasing the bismuth content beyond 1.5%, the degradation rate increased. It can be concluded that the rate of degradation is higher (rate constant value of 0.1176 min^{-1}) with Cat-B compared to all other catalysts synthesized. Comparing the photocatalytic activity of Cat-A with Cat-B; Cat-E with Cat-G; Cat-H with Cat-I, it was found that the US-WI catalysts showed higher photocatalytic activity than the catalysts synthesized by sol-gel method. This is attributed to the uniform particle sizes of the wet impregnated catalysts facilitating better accessibility of active metals on the surface, which is evident from the morphology analysis (Fig. 4). It is also reported in the literature that the Bi modified TiO_2 increased the photocatalytic activity due to high surface area and reduced recombination rate and increased absorption of visible light [27]. The high photocatalytic activity of the bi-metallic catalyst is ascribed to the defects of Ti interstitials, O vacancies, H inclusions and these surface defects caused due to the metal doping on the surface, traps the holes and electrons reducing the probability of recombination rate [28]. Silver narrows the band gap energy with a Fermi level having lower energy than the conduction band of TiO_2. Moreover, the boosted performance of the Bi-Ag catalyst is attributed to creating a Z-scheme like structure providing the new electron transfer mediator and ensuring the effective separation of photogenerated charge carriers [20].

2-3. Effect of Initial Dye Concentration

The bi-metallic catalyst Cat-B, which was found to be promising in terms of catalytic activity, was further studied to determine the optimum process conditions. The effect of initial dye concentration on the degradation rate was studied by varying the Rh-B initial concentration from 10 ppm to 45 ppm at pH=7 and a catalyst loading of 60 mg/L. The obtained results shown in Fig. 7 demonstrate that the degradation decreased from 100% to 68% with increasing dye concentration from 10 to 45 ppm. Also, the observed rate constant decreased from 0.1186 min^{-1} to 0.0195 min^{-1} with increasing concentration over the same range. The results are in-line with earlier reported studies in which the downtrend is attributed to several reasons such as *a*) hindering the diffusion of hydroxyl radicals to the TiO_2 surface due to increased pollutant concentration which led to decrease in the formation of reactive species, and *b*) higher concentrations of dye absorb higher number of photons, which decreases the availability of photons to activate the photocatalyst leading to lower generation of oxidizing species [24]. It is also clear that in all the cases studied, there was a rapid degradation within the first 25 min followed by a slow degradation rate in

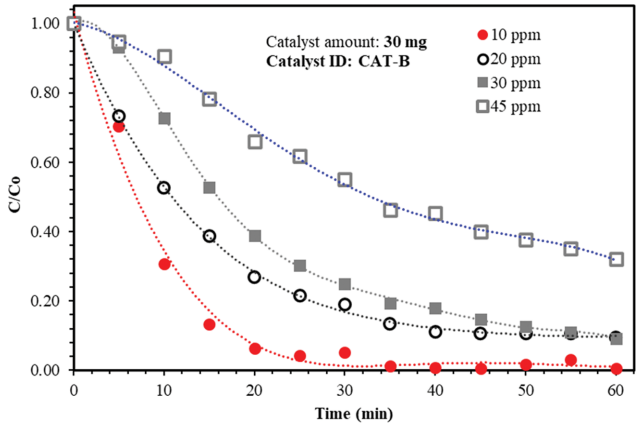

Fig. 7. Concentration effect of Rh-B dye on the degradation with CAT-B [Experimental conditions: T=25 °C, pH=7, agitation= 800 rpm; catalyst amount=30 mg; feed volume=500 ml].

the later stage. This is due to the high initial oxidant activity due to which the dyes are degraded to smaller molecules that act as hydroxyl radical scavengers, reducing their availability for dye degradation. Maximum degradation of >95% was achieved in 60 min with initial feed concentration till 30 ppm and further increasing the concentration led to a slower degradation rate.

2-4. Effect of Catalyst Loading

The effect of varying amounts of catalyst in the range of 30-150 mg was studied with initial Rh-B concentration of 45 ppm using the bimetallic catalyst (Cat-B), and the obtained results are shown in Fig. 8. It was observed that with an increase in catalyst loading from 30 mg to 150 mg, the degradation increased from 68% to 90% with a corresponding increase in rate constant from 0.02 min^{-1} to 0.04 min^{-1}. The increased degradation is attributed to the higher accessibility of TiO_2 surface and greater release of photons with an increase in the quantity of the catalyst. However, it was also seen that the degradation did not improve significantly beyond the catalyst loading of 120 mg established as the optimum amount. Similar observations of optimum catalyst loading were reported in the literature which depend on the catalyst size distribution, catalyst type, pollutant concentration and reactor configurations which determine the generation of free radicals [29].

Increasing the catalyst loading will eventually increase the number of active sites on the surface there by facilitating the production of increased hydroxyl and superoxide radicals, which in turn increase the degradation rate. However, above the optimum catalyst loading, the degradation rate was found to be decreased, which is attributed to the interception of the light by the suspension as well as the excess catalyst preventing the illumination [30,31]. From a technology deployment perspective, it is important to have the low catalyst loading with high activity and long catalyst life that is reported in this study (See comparison given in Table S1).

2-5. Effect of pH

The pH of the dye solution strongly influences the degradation rate as it controls the interaction between the photocatalyst and the dye molecules. The pKa value of Rh-B was around 3.1, but the working best condition reported by several authors was found to be 5. The effect of pH on the degradation was studied by varying pH from 3 to 10 using Cat-B (60 mg/L). From Fig. 9, it was seen that the final percentage degradation achieved with different pH solutions around 30 min was more or less similar to minimal changes in the initial rates of degradation. The degradation rate of different dyes (cationic/anionic) behaves differently under photocatalytic conditions, depending on their pKa values [32]. Byrappa et al. [33], noticed low rate constant at a pH of 7, which was found to increase with acidic as well as alkaline pH values. In another study, low photocatalytic degradation of Rh-B was reported with strong acidic and alkaline conditions [34]. On the contrary, Nagaraja et al. [35] reported alkaline conditions favoring maximum degradation rates at pH 12. Industrial effluents are typically neutral (neutralization tank) and the photocatalytic degradation under such conditions is economically viable with minimal chemical dosing requirement. In this study, the dye degradation was unaffected by the solution pH and can be applied over a wide range of pH including desired neutral conditions.

2-6. Degradation of Different Dyes under Visible Light

For a cost-effective process, photocatalyst needs to be highly

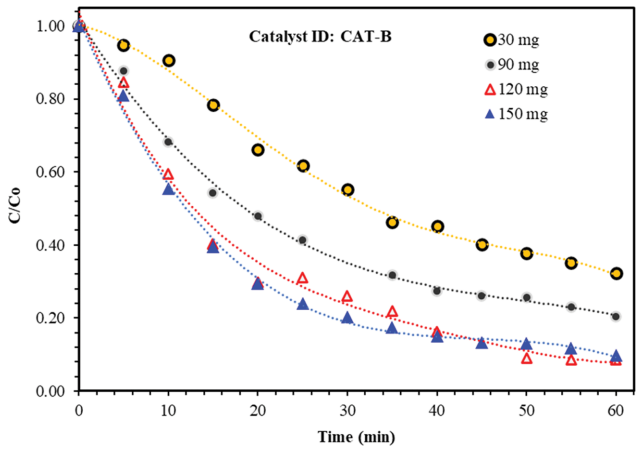

Fig. 8. Effect of catalyst loading [Experimental conditions: T=25 °C, pH=7, agitation=800 rpm; feed concentration=45 ppm; feed volume=500 ml].

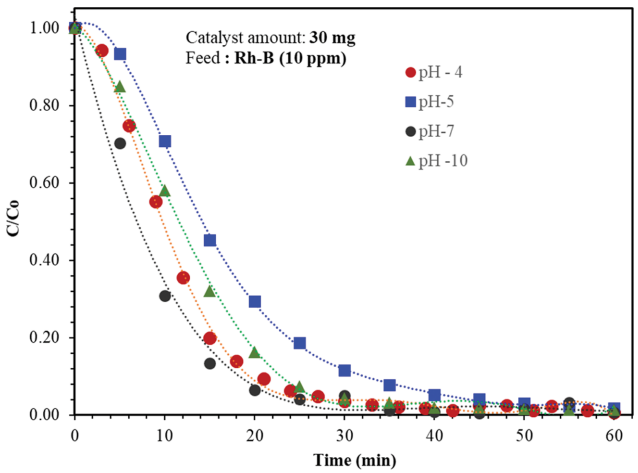

Fig. 9. Effect of pH on the degradation rate of Rh-B.

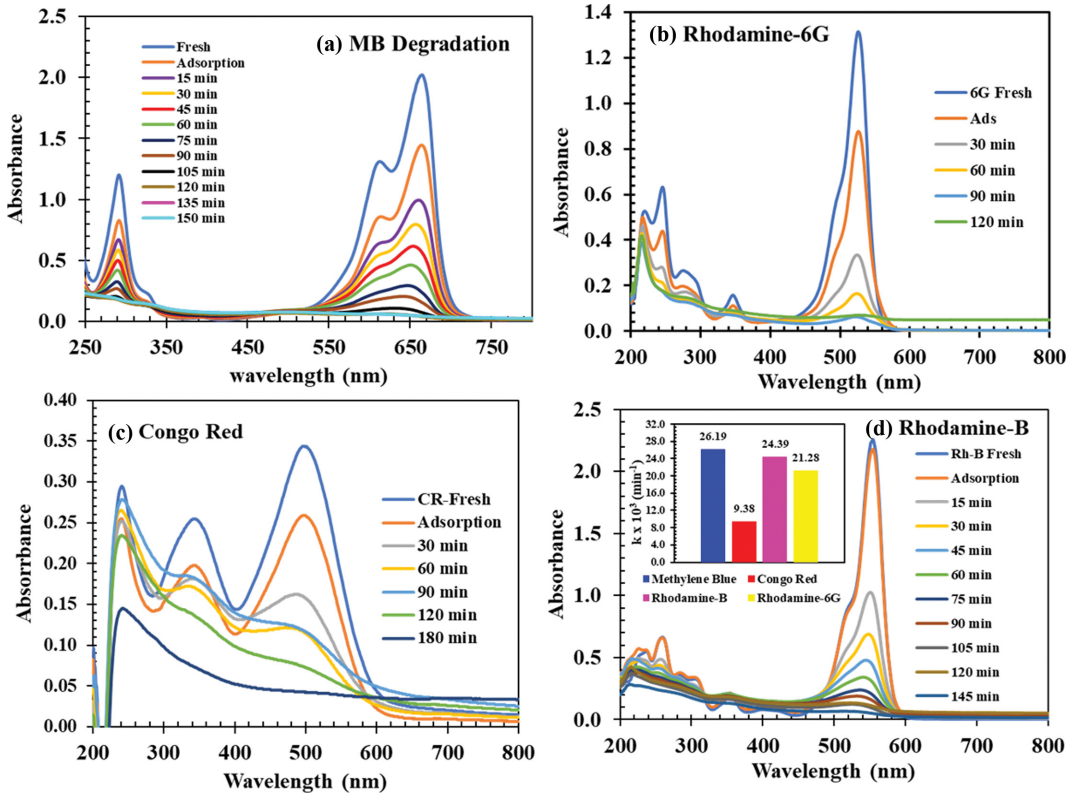

Fig. 10. Photocatalytic degradation of different dyes [(a) Methylene blue (b) Rhodamine-6G, (c) Congo Red, (d) Rhodamine - B] under visible light conditions [Experimental conditions: T=25 °C, pH=7, agitation=800 rpm; dye concentration=10 ppm; catalyst amount - 30 mg; catalyst- Cat-B, feed volume=500 ml; visible sunlight].

active and stable in completely degrading any type of pollutants under visible light conditions and possibly in a shorter treatment time. To investigate the effectiveness of the catalyst, photocatalytic studies with different dyes (MB, Rh-6G CR, Rh-B) were carried out in visible sunlight conditions with initial feed concentration of 10 ppm and a catalyst amount of 30 mg. The results illustrated in Fig. 10 confirm that the bimetallic Bi-Ag catalyst was highly effective in degrading different dyes under visible sunlight in a short span. About 90% degradation was achieved with Methylene blue after 120 min with a degradation rate constant of 0.026 min^{-1}. With Rh-B, it was observed that ~54% of degradation was obtained within 15 minutes of exposure to sunlight that increased to 90% in 75 min with a degradation rate constant of 0.02439 min^{-1}. While, for Rh-6G and CR solutions, 90% degradation was attained within 90 min of sunlight exposure, having a degradation rate constant of 0.0212 min^{-1} and 0.009 min^{-1}, respectively. The degradation rate of different dyes followed the order of MB>Rh-B>Rh-6G>CR, as shown in Fig. 10(d). It is also clear from the figure that maximum degradation was achieved within 90 min for all the dyes. Rh-B and Rh-6G are identical with respect to molecular weight but with different end groups and hence the degradation rates would be more or less similar. The rate of MB degradation was found to be higher than the CR, which agrees well with the literature [36]. Comparatively, it was observed that the chemical structure of MB lends itself more to oxidation by hydroxyl radicals than CR. Moreover, it is possible that MB absorbs less UV light, making more photons available to impinge on to the catalyst, which promotes the hydroxyl radical generation.

Additional experiment was also carried with pure TiO_2 for the degradation of Rh-B dye under identical conditions and the obtained results were compared with Cat-B to check the effect of metal doping. The rate constant obtained with pure TiO_2, and Cat-B was found to be 0.0114 and 0.0244 min^{-1}, indicating high photocatalytic activity with metal doped TiO_2. Natarajan et al. also reported higher efficacy for the doped catalysts with 97% and 100% degradation of Rh-B dye seen in 4 h and 3 h using TiO_2 nanotubes and 0.5 wt% Bi doped TiO_2 nanotubes respectively [9]. Our results are very promising in terms of high catalyst efficacy in the photocatalytic degradation of different dyes achieved within shorter duration (~90 min) and minimal catalyst loadings (60 mg/l) under visible light conditions making the process economically viable for scale up operations.

2-7. Catalyst Reusability

Catalyst reusability is an important parameter that significantly affects treatment costs. The catalyst reusability was studied for five cycles in the photocatalytic reactor, and the obtained results are shown in Fig. 11. Since the amount of catalyst used was very low (here: 200 mg/L) and due to complete dispersion of the catalyst in the feed solution, it was difficult to recover the catalyst completely after each cycle. Hence, the reusability of the catalyst was tested by directly adding specific amount of dye (calculated based on the final concentration of the left solution) to the treated effluent after each

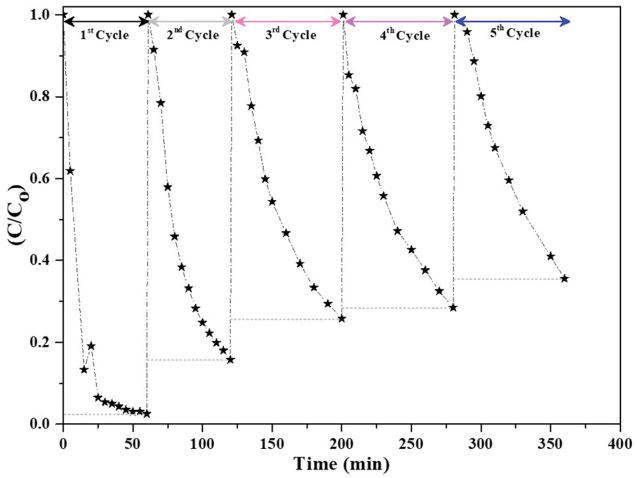

Fig. 11. Catalyst reusability test [Experimental conditions: T=25 °C; pH=7; agitation=800 rpm; dye concentration=20 ppm; catalyst amount=100 mg; catalyst=Cat-B; feed volume=500 ml; UV reactor].

cycle, bringing the initial feed concentration to 20 ppm. In the first cycle, the dye was almost completely degraded with a conversion of 96% in 30 min. Whereas, in the subsequent cycles lower conversions of 84%, 67%, 62% and 55% were noticed after 60 min of reaction time for 2nd, 3rd, 4th and 5th cycles respectively. The declining trend of the photocatalytic activity is attributed due to the following reasons: *i*) blockage of active sites due to permanent adsorption on the catalyst surface, and *ii*) due to the presence of intermediate products being more recalcitrant and may even act as hydroxyl radical scavenger. Overall, the catalyst was found to be significantly active enough even after five cycles, showing good recyclability considering the fact that the treated effluent containing catalyst was used for the other cycles. However, future work in the catalyst development area must be aimed towards improving catalyst life, regeneration ability and also application in a continuous operation.

2-8. Mechanistic Degradation Pathway of Rh-B Dye

It is important to understand the mechanism of photocatalytic degradation of dyes in UV/visible light region that helps in devising better strategies for catalyst development for complete mineralization of intermediates and final products of dye degradation process. This is usually carried out by the aqueous effluent analysis to determine the intermediate and final degradation products. Herein, we have a proposed a plausible mechanism for the photocatalytic degradation of Rh-B based on earlier studies [37] as illustrated in Fig. 12.

Usually, two competitive processes proceed during the photoreaction such as N-deethylation and degradation of dye chromophore. Among these two steps N-deethylation products (N, N-diethyl-N′-ethylrhodamine (DER), N-ethyl-N′-ethylrhodamine (EER), N, N-diethylrhodamine (DR), N-ethylrhodamine (ER)) are supposed to exist in small quantities and cleavage of the chromophore structure of the Rh-B is considered to be more dominant in the photoreaction. Most of the N-deethylation (step wise) processes leads to the formation of nitrogen centered radical, while degradation of dye chromophore leads to the generation of carbon centered radical. The formation of the nitrogen centered or carbon centered radical is determined by the modes of adsorption of the dye molecule on the catalyst surface. It is usually expected

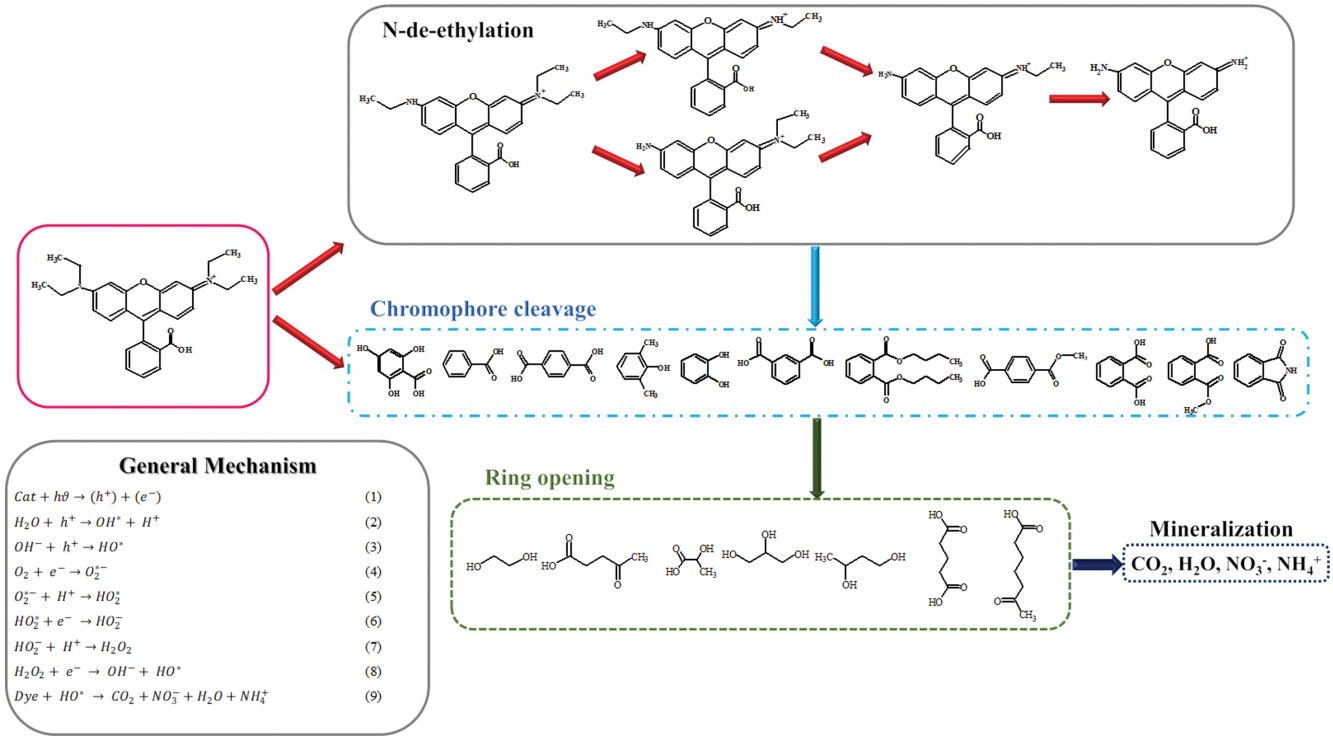

Fig. 12. Schematic representation of the photocatalytic degradation pathways of Rh-B [37].

that the dye molecule adsorbs on the catalyst surface due to its positively charged diethylamine function. The first step involves N-deethylation processes where the N-deethylated products successively undergo decomposition during the photooxidative process. On the other hand, the facile cleavage of the dye chromophore proceeds throughout the degradation process where the photogenerated hydroxyl radical directly attacks the carbon-centered radical leading to decolorization. During this degradation process, several oxidation intermediate products (*e.g.*, adipic acid, phthalic acid, isophthalic acid, terephthalic acid) are formed, which further degrades into smaller compounds (*e.g.*, ethane-1, 2 diol, butane-1, 3 diol, propane-1,2 3-triol) and so forth eventually leading to the complete mineralization products such as CO_2, H_2O and NH_3. Overall, the question of which radical formation takes place (nitrogen-centered or carbon-centered) dictates the dominant pathway, but often both N-dethylation and chromophore cleavage steps occur during the photoreaction and the quantity of these intermediate compounds formed during the process plays a vital role in the mechanism.

A simplified general mechanism is illustrated in Fig. 12, in which the electrons in the conduction band of the catalyst get excited to the valence band creating holes (reaction 1), where both charge carriers migrate to the catalyst surface. Further, upon UV-light irradiation, hydrogen ions would be generated from water molecules (reaction 2). The valence band holes further react with hydroxyl groups (OH^-) on the catalyst surface, producing hydroxyl radicals (HO*) (reaction 3) and the electrons with dissolved oxygen molecules produce super oxide radical anion (O_2^{*-}) (reaction 4). The formed superoxide anions may further generate hydroxyl radicals with generated H^+ ions and electrons (reaction 5-8) or may attack organic molecules directly. The generated hydroxyl radicals degrade the organic pollutants present in wastewater (Fig. S1 depicts the schematic representation). However, during the degradation process several reaction intermediates are produced that can act as hydroxyl radical scavenger, suppressing the degradation rate. Therefore, an efficient catalyst must not only be able to produce maximum radicals but also be able to suppress the recombination rates.

CONCLUSIONS

Mono and bi-metallic doped TiO_2 catalysts with different loadings of Bi and Ag were prepared, characterized, and successfully tested for the degradation of synthetic dyes. Ultrasound assisted wet impregnated catalysts were found to be highly efficient in the photocatalytic degradation of dyes when compared to the sol gel method. An optimum loading of 0.5 : 0.5 wt% Bi-Ag/TiO_2 was found to be highly effective in achieving complete dye degradation both under UV and visible light irradiation at low catalyst loading (60 mg/L) and short treatment time. The best performing Bi-Ag/TiO_2 catalyst was further studied to optimize the process conditions, such as catalyst loading, initial dye concentration and initial feed pH solution. The optimum catalyst loading was found to be 120 mg for a 45 ppm Rh-B feed solution. With increase in the catalyst loading beyond 120 mg, no significant increase in rate of degradation was noticed. The optimum feed concentration was found to be 30 ppm for a catalyst loading of 30 mg. With increase in feed concentration beyond 30 ppm, the rate of degradation was significantly reduced, and the final degradation achieved in 60 min was lower. The initial feed pH was found to have a minimal effect on the overall degradation. The photocatalytic effect of Ag doped on TiO_2 (Cat-G), and bimetallic Ag-Bi doped on TiO_2 (Cat-B) catalysts was higher in comparison with all other catalysts assessed using the extent of degradation and rate constant values. The photocatalytic performance of Cat-B was tested in visible light using different dyes and almost complete degradation was achieved for all the dyes within 100-120 minutes. The high photocatalytic activity is ascribed to the concentration of defects due to disordered phase and reducing the recombination of electrons and holes. Recyclability experiments indicate that the bi-metallic catalyst exhibits a good stability and reusability. Indeed, more studies are required to check the photocatalytic performance in a continuous scale operation, evaluating the hydroxyl production and elucidating the reaction mechanism by analyzing the intermediates produced from the liquid effluent.

ACKNOWLEDGEMENTS

The authors (NC, PRG) would like to acknowledge the Indian National Academy of Engineering (INAE) for mentorship program of engineering faculty. The authors would like to thank Manipal University Jaipur (MUJ) for providing access to the Central Analytical Facilities (CAF) and Sophisticated Analytical Instrumentation Facility (SAIF). One of the authors (AGC) would also like to acknowledge the endowment seed grant (EF/2017-18/QE04-06) provided by the University.

SUPPORTING INFORMATION

Additional information as noted in the text. This information is available via the Internet at http://www.springer.com/chemistry/journal/11814.

REFERENCES

1. E. COMMISSION, Publ. Off. Eur. Union (2014).
2. N. N. Mahamuni and Y. G. Adewuyi, *Ultrason. Sonochem.*, **17**, 990 (2010).
3. Y. G. Adewuyi, *Environ. Sci. Technol.*, **39**, 10 (2005).
4. S. Bagwasi, B. Tian, J. Zhang and M. Nasir, *Chem. Eng. J.*, **217**, 108 (2013).
5. F. Fresno, R. Portela, S. Suárez and J. M. Coronado, *J. Mater. Chem. A*, **2**, 2863 (2014).
6. X. Wang, Y. Wang and Z. Yan, *Int. J. Photoenergy*, **2014**, 1 (2014).
7. M. K. Seery, R. George, P. Floris and S. C. Pillai, *J. Photochem. Photobiol. A Chem.*, **189**, 258 (2007).
8. M. A. Behnajady and H. Eskandarloo, *Chem. Eng. J.*, **228**, 1207 (2013).
9. T. S. Natarajan, K. Natarajan, H. C. Bajaj and R. J. Tayade, *J. Nanoparticle Res.*, **15**, 1 (2013).
10. S. I. Mogal, V. G. Gandhi, M. Mishra, S. Tripathi, T. Shripathi, P. A. Joshi and D. O. Shah, *Ind. Eng. Chem. Res.*, **53**, 5749 (2014).
11. N. Sobana, M. Muruganadham and M. Swaminathan, *J. Mol. Catal.*

A Chem., **258**, 124 (2006).
12. H. Zhao, F. Tian, R. Wang and R. Chen, *Rev. Adv. Sci. Eng*., **3**, 3 (2014).
13. Y. Wu, G. Lu and S. Li, *J. Phys. Chem. C*, **113**, 9950 (2009).
14. S. Sajjad, S. A. K. Leghari, F. Chen and J. Zhang, *Chem. - A Eur. J*., **16**, 13795 (2010).
15. J. Xu, M. Chen and D. Fu, *Appl. Surf. Sci*., **257**, 7381 (2011).
16. K. Atacan, N. Güy and M. Özacar, *Colloids Interface Sci. Commun*., 40 (2021).
17. N. Güy, K. Atacan, İ. Yıldırım and M. Özacar, *J. Mol. Liq*., 326 (2021).
18. A. Chachvalvutikul, T. Luangwanta, S. Pattisson, G. J. Hutchings and S. Kaowphong, *Appl. Surf. Sci*., 544 (2021).
19. V. K. Landge, S. H. Sonawane, M. Sivakumar, S. S. Sonawane, G. Uday Bhaskar Babu and G. Boczkaj, *Sustain. Energy Technol. Assessments*, **45**, 101194 (2021).
20. C. Zhang, W. Chen, D. Hu, H. Xie, Y. Song, B. Luo, Y. Fang, W. Gao and Z. Zhong, *Green Energy Environ*. (2021).
21. S. Rengaraj and X. Z. Li, *Int. J. Environ. Pollut*., **27**, 20 (2006).
22. V. Vetrivel, K. Rajendran and V. Kalaiselvi, *Int. J. ChemTech Res*., **7**, 1090 (2015).
23. F. M. Bautista, J. M. Campelo, A. Garcia, D. Luna, J. M. Marinas, M. C. Moreno, A. A. Romero, J. A. Navio and M. Macias, *J. Catal*., **173**, 333 (1998).
24. S. Rajoriya, S. Bargole, S. George, V. K. Saharan, P. R. Gogate and A. B. Pandit, *Sep. Purif. Technol*., **209**, 254 (2019).
25. P. S. Sathish Kumar, R. Sivakumar, S. Anandan, J. Madhavan, P. Maruthamuthu and M. Ashokkumar, *Water Res*., **42**, 4878 (2008).
26. P. C. L. Muraro, S. R. Mortari, B. S. Vizzotto, G. Chuy, C. dos Santos, L. F. W. Brum and W. L. da Silva, *Sci. Rep*., **10**, 1 (2020).
27. S. Sood, S. K. Mehta, A. Umar and S. K. Kansal, *New J. Chem*., **38**, 3127 (2014).
28. M. Zimbone, M. A. Buccheri, G. Cacciato, R. Sanz, G. Rappazzo, S. Boninelli, R. Reitano, L. Romano, V. Privitera and M. G. Grimaldi, *Appl. Catal. B Environ*., **165**, 487 (2015).
29. P. R. Gogate and A. B. Pandit, *AIChE J*., **50**, 5 (2004).
30. S. Chakrabarti and B. K. Dutta, *J. Hazard. Mater*., **112**, 269 (2004).
31. U. G. Akpan and B. H. Hameed, *Appl. Catal. A Gen*., **375**, 1 (2010).
32. U. G. Akpan and B. H. Hameed, *J. Hazard. Mater*., **170**, 2 (2009).
33. K. Byrappa, A. K. Subramani, S. Ananda, K. M. Lokanatha Rai, R. Dinesh and M. Yoshimura, *Bull. Mater. Sci*., **29**, 433 (2006).
34. G. Sharma, D. D. Dionysiou, S. Sharma, A. Kumar, A. H. Al-Muhtaseb, M. Naushad and F. J. Stadler, *Catal. Today*, **335**, 437 (2019).
35. R. Nagaraja, N. Kottam, C. R. Girija and B. M. Nagabhushana, *Powder Technol*., **215-216**, 91 (2012).
36. M. Z. Bin Mukhlish, F. Najnin, M. M. Rahman and M. J. Uddin, *J. Sci. Res*., **5**, 301 (2013).
37. K. Yu, S. Yang, H. He, C. Sun, C. Gu and Y. Ju, *J. Phys. Chem. A*, **113**, 10024 (2009).

Supporting Information

Highly efficient bi-metallic bismuth-silver doped TiO_2 photocatalyst for dye degradation

Nandana Chakinala*, Parag Ratnakar Gogate, and Anand Gupta Chakinala*,†**

*Department of Chemical Engineering, Manipal University Jaipur, Dehmikalan, Jaipur-303007, Rajasthan, India
**Department of Chemical Engineering, Institute of Chemical Technology, Mumbai-400019, Maharashtra, India
(*Received 29 April 2021 • Revised 14 June 2021 • Accepted 2 July 2021*)

1. Comparison of Experimental Data with Literature

Table S1 summarizes a detailed literature overview of photocatalytic degradation of Rh-B. This table clearly illustrates that the results obtained in this study are very significant in nature with respect to the conversions achieved within shorter duration and with limited amount of catalyst loading under day light conditions.

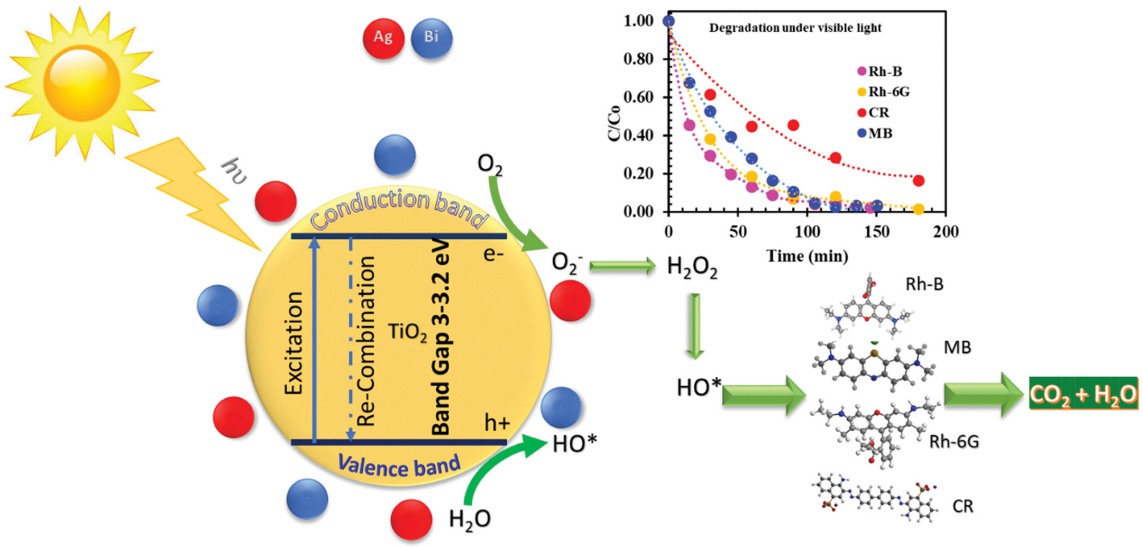

Fig. S1. Schematic of photocatalytic degradation of Rh-B over catalyst surface.

Table S1. Literature overview of photocatalytic degradation of Rh-B dye

Dye	Feed conditions	Reactor details	Catalyst	Loading	Conversion	Time	Ref
Rh-B	10 mg/L	500 W Xe lamp as light source	Bi_2S_3-sensitized BiOCl (Bi_2S_3/BiOCl)	0.6 g/L	98%	120 min	[1]
Rh-B	20 mg/L	Natural sunlight conditions, light intensity: $34\times10^3\pm100$ lx	Sr/Ce/AC	0.3 g/L	91%	120 min	[2]
Rh-B	10 mg/L, 50 mL solution	UV provided by 125 W high pressure mercury vapor lamp	TiO_2	1 g/L	96%	40 min	[3]
Rh-B	30 mg/L, 450 mL solution	Low pressure mercury lamp 11 W with the aid of 1 mM of peroxy Disulpulfate	(LaZF@rGO)	0.25 g/L	100% with PDS	60 min	[4]

Table S1. Continued

Dye	Feed conditions	Reactor details	Catalyst	Loading	Conversion	Time	Ref
Crystal violet dye	30 mg/L, 150 mL solution	UV lamp with intensity 2,000 W/cm^2	2 mol% Fe doped TiO_2 and 2 mol% Ce doped TiO_2 (US)	0.2 g/L	84% with Ce-TiO_2 77% with Fe-TiO_2	120 min	[5]
Rh-B	25 mg/L, 90 mL solution	50 W high pressure mercury lamp with light intensity 2.85 mW/cm^2	Ag/In_2O_3-TiO_2	1.67 g/L	100%	45 min	[6]
Rh-B	10 mg/L	150 W tungsten halogen lamp	La_2O_3/Ag_3VO_4	0.5 g/L	100%	180 min	[7]
Rh-B	10 mg/L	500 W Xenon Lamp	TiO_2/MgZnAl	1 g/L	94%	9 h	[8]
Rh-B	100 mL, 1×10^{-5} M	500 W Xenon Lamp	Bi_2WO_6	0.5 g/L	98%	60 min	[9]
Rh-B	7 L feed solution	Single UV tube, LUXRAM make with power of 11 W	TiO_2	2 g/L	40%	150 min	[10]
Rh-B	100 ml of 50 μM solution	250 W high pressure mercury lamp	SnO_2 embedded SBA-15 mesoporous silica	0.75 g/L	90%	10 h	[11]
Rh-B	10 mg/L, 50 mL solution	350 W Xe lamp with intensity 18 mW/cm^2	$BiOCl_xI_{1-x}$ structures with x=0.75	0.2 g/L	98%	60 min	[12]
Rh-B	6 mg/L	150 W Halide lamp	$Co_{0.6}Mg_{0.4}Fe_2O_4$	0.31 g/L	99%	250-300 min	[13]
Rh-B, Malachite green, Methylene blue	2.08×10^{-5} M; 25 ml solution	UV-LED; 10-12 mW	P25 (TiO_2)	1.6 g/l	>95%	180 min	[14,15]
Rh-B	33 mg/l of 50 ml solution	Sunlight	ZnO	4 g/l	97%	180 min	[16]
Rh-B	10 mg/l of 100 ml solution	125 W Lamp	ZnO powder	2 g/l	100%	80 min	[17]
Rh-B	25 mg/l of 100 ml solution	Visible light	$BiFeO_3$	0.5 g/l	100%	35-40 min	[18]
Rh-B	5-25 mg/l of 250 ml solution	Osram Ultra-Vitalux lamp (300 W)	Bi_2WO_6-TiO_2	n.a.	100%	~90 min visible light ~30 min under UV lamp	[19]
Rh-B	10 mg/l of solution	Xenon arc lamp	ZnO	0.15 g	95%	80 min	[20]
Rh-B	10 mg/l of solution	UV-Vis/Visible sunlight condition	BiAg/TiO_2	0.06 g/L	100%	<30 min with UV lamp ~100 min in visible light	This study

BIBILIOGRAPHY

1. J. Cao, B. Xu, H. Lin, B. Luo and S. Chen, *Catal. Commun.*, **26**, 204 (2012).
2. G. Sharma, D. D. Dionysiou, S. Sharma, A. Kumar, A. H. Al-Muhtaseb, M. Naushad and F. J. Stadler, *Catal. Today*, **335**, 437 (2019).
3. T. Aarthi and G. Madras, *Ind. Eng. Chem. Res.*, **46**, 7 (2007).
4. B. M. Jun, S. S. Elanchezhiyan, Y. Yoon, D. Wang, S. Kim, S. Muthu Prabhu and C. M. Park, *Chem. Eng. J.*, **393**, 124733 (2020).
5. S. R. Shirsath, D. V. Pinjari, P. R. Gogate, S. H. Sonawane and A. B. Pandit, *Ultrason. Sonochem.*, **20**, 277 (2013).
6. X. Yang, L. Xu, X. Yu and Y. Guo, *Catal. Commun.*, **9**, 1224 (2008).
7. H. Xu, H. Li, G. Sun, J. Xia, C. Wu, Z. Ye and Q. Zhang, *Chem. Eng. J.*, **160**, 33 (2010).
8. G. Zhao, J. Zou, C. Li, J. Yu, X. Jiang, Y. Zheng, W. Hu and F. Jiao,

J. Mater. Sci. Mater. Electron., **29**, 7002 (2018).
9. H. Fu, C. Pan, W. Yao and Y. Zhu, *J. Phys. Chem. B*, **109**, 22432 (2005).
10. K. P. Mishra and P. R. Gogate, *J. Environ. Manage*., **92**, 1972 (2011).
11. N. R. Srinivasan and R. Bandyopadhyaya, *Micropor. Mesopor. Mater*., **149**, 166 (2012).
12. J. Xie, Y. Cao, D. Jia and Y. Li, *J. Colloid Interface Sci*., **503**, 115 (2017).
13. M. Sundararajan, L. John Kennedy, P. Nithya, J. Judith Vijaya and M. Bououdina, *J. Phys. Chem. Solids*, **108**, 61 (2017).
14. K. Natarajan, T. S. Natarajan, H. C. Bajaj and R. J. Tayade, *Chem. Eng. J*., **178**, 40 (2011).
15. T. S. Natarajan, M. Thomas, K. Natarajan, H. C. Bajaj and R. J. Tayade, *Chem. Eng. J*., **169**, 126 (2011).
16. K. Byrappa, A. K. Subramani, S. Ananda, K. M. Lokanatha Rai, R. Dinesh and M. Yoshimura, *Bull. Mater. Sci*., **29**, 433 (2006).
17. R. Nagaraja, N. Kottam, C. R. Girija and B. M. Nagabhushana, *Powder Technol*., **215-216**, 91 (2012).
18. T. Soltani and M. H. Entezari, *Chem. Eng. J*., **223**, 145 (2013).
19. S. Murcia López, M. C. Hidalgo, J. A. Navío and G. Colón, *J. Hazard. Mater*., **185**, 1425 (2011).
20. Q. I. Rahman, M. Ahmad, S. K. Misra and M. Lohani, *Mater. Lett*., **91**, 170 (2013).